ISSN : 0974 - 7435 Volume 10 Issue 19

2014

BioTechnology

An Indian Journal

FULL PAPER

BTAIJ, 10(19), 2014 [11715-11721]

Enhancement of image quality with scatter correction for Cone Beam CT

Shipeng Xie[1*], Ruiju Yan[1], Mingchen Ding[2], Wenze Shao[1], Xiaogang Cheng[1], Hu Zhu[1]

[1]Nanjing University of Posts and Telecommunications, College of Telecommunications & Information Engineering, Nanjing 210003, Jiangsu, (PEOPLES REPUBLIC OF CHINA)

[2]Nanjing Municipal Bureau of Statistics, Nanjing 210019, Jiangsu, (PEOPLES REPUBLIC OF CHINA),

E-mail : Shipeng Xie, Email:xie@njupt.edu.cn

ABSTRACT

The scattering phenomenon has an important influence on the reconstructed image in Cone Beam CT (CBCT) imaging systems, and is a long-lasting research topic on CBCT. Focusing on the scatter artifacts in the cone beam CT system, we proposed a powerful scatter correction method using a scatter detecting blocker (SDB) between the X - ray source and the tested object, and then educed the scatter correction algorithm based on the Beer theorem. The result shows that our proposed method can effectively reduce the scatter artifacts and increase the quality of the reconstructed slice image. Our approach reduce the magnitude of cupping from 42.3% to 1.3% and increase the CNR from1.75 to 2.35. This method is computationally efficient, easy to implement, and provides scatter correction using a single scan acquisition without the loss of real-time imaging capabilities.

KEYWORDS

Scatter correction; Compton scatter; Cone beam CT.

INTRODUCTION

An x-ray system with a large area detector, as commonly used for cone-beam computed tomography (CBCT), is more susceptible to scatter-related artifacts. To alleviate this problem, various correction methods using software-based[1–6], hardware-based[7–11], or combined hybrid approaches[13-14] have been proposed in the literature. Approaches proposed to estimate the spatial distribution of scatter on the detector plane includes model-based analytical calculation[15-16]and Monte Carlo simulation[17]. Generally speaking, the model in the analytical scheme is usually regular in geometry and homogeneous in radiation properties[15], and thus the estimated scatter may not reflect the real situation. Collimator- and blocker-shaded schemes are based on the fact that scatter distribution in space is rather smooth so that it could be reconstructed by knowing the scatter in some regions. However, other types of noise and artifacts in the imaging system could cause difficulty in estimating the algorithm parameters for reconstruction and thus resulting in either under- or overcorrection of scatter, although the difficulty can be somewhat alleviated by adding more shaded regions. Scatter estimation from Monte Carlo simulation is accurate if the information on the scattering medium is known from, for example, computed tomography CT. However, formidably heavy computation in Monte Carlo scatter estimation hinders its real life applications. So in this paper, we propose an improved method to correct for scatter and gain information on the scattering object at the same time.

METHOD

The system geometry and implementation

Figure 1 shows the system geometry with the insertion of the SDB. In this new scatter correction method, a SDB was added between the X - ray source and the tested object. In addition, the method was evaluated on tabletop CBCT systems.

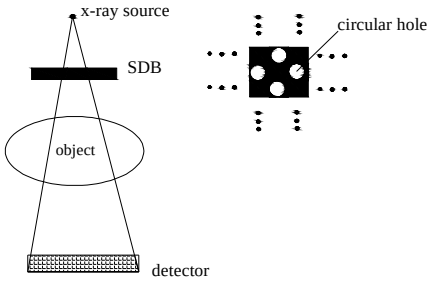

Figure 1 : Geometric configuration of the x-ray system with the insertion of the SDB.

A 130 mm×130 mm SDB with 30×30 holes made by aluminium is shown in Figure 2, which was designed to investigate the impact of SDB on the scatter correction performance. The diameter of the circular hole is 2 mm, and the distance between the two hole's center is 4mm. The base thickness of the SDB is 2 mm. As in Figure 1, the SDB is placed between the object and the X-ray source. In our experiments, the distance between X-ray source and the object is 1000 mm, between X-ray source and the SDB is 230 mm, while between X-ray source and detector is 1400 mm.

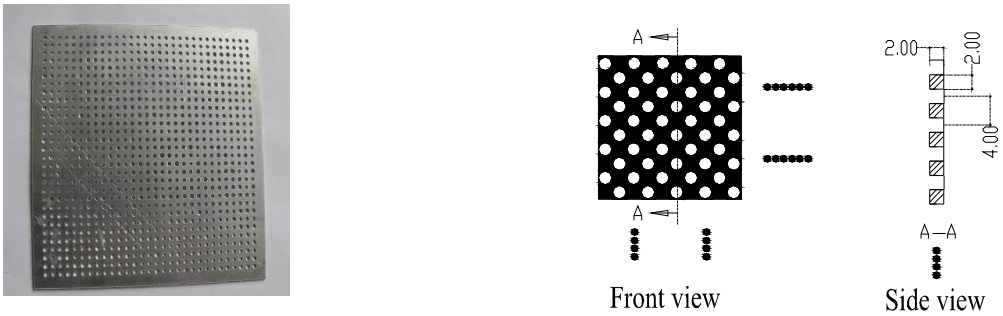

Figure 2 : The SDB. Unit: mm

The scatter correction algorithm for the modified system with the insertion of the SDB is divided into the following steps, embedded in the conventional image processing stage of x-ray CT:

Step 1 Do two air pre-scans with and without the SDB, and estimate the blocker hole shadow position.

Step 2 Process the air scan image with the SDB used to obtain an attenuation coefficient β , which is the ratio of the scan image with and without SDB.

Step 3 Acquire projection images of the object with the SDB in place.

Step 4 For each projection image:

Step 4.1 downsample the projection *P* at the centers of the blocker hole shadows;

Step 4.2 using the border upon blocker shadows as C_1 and C_2 which is defined in Section Ⅱ.B, and then computer the scatter fluence S .

Step 4.3 upsample the scatter fluence S . using cubic interpolation; this provides an estimate of the whole-field scatter estimate S_e .

Step 4.4 do subtraction P - S_e

Step 4.5 weight it by matrix β .

Step 5 Reconstruct using the processed projection images.

The algorithm of scatter estimation

As shown in Figure 3, the SDB is placed between the object and the X-ray source. I_0 is the fluence of the incident X-ray. S_1 , S_2 are the scatter fluence through the object. After the attenuation of the SDB, the photons fluence are I_{11} , I_{21} . I_{12} , I_{22} are the photons fluence through the object. C_1 , C_2 are the measured fluence which arrive in the detector ($C_1 = I_1 + S_1$, $C_2 = I_2 + S_2$).

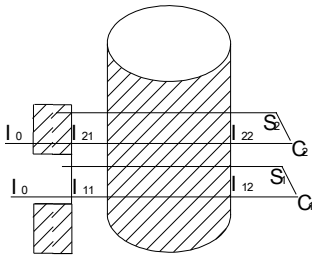

Figure 3 : Scatter correction algorithm diagram

The BEER theorem is given by:

$$I_{11} = I_0 , \quad \textbf{(1)}$$

$$I_{21} = I_0 e^{-u_1 d} , \quad \textbf{(2)}$$

here $d = 2mm$ is the thickness of the SDB and u_1 is the attenuation coefficient of the x-ray beam in the SDB. As the low-frequency components still dominate in the scatter distribution, so $S_2 = S_1$ in a small area.

$$I_{22} = C_2 - S_2 = I_{21} e^{-u_2' l'} , \quad \textbf{(3)}$$

$$I_{12} = C_1 - S_1 = I_{11} e^{-u_2 l} , \quad \textbf{(4)}$$

here l and l' are the thicknesses of the object. u_2 and u_2' are the attenuation coefficient of the x-ray beam in the object. To this problem, we noticed that the projections of most objects vary continuously in most space. That is to say, we could find some shaded pixels and their adjacent without-shade pixels which have the nearly identical u_2 and u_2' . In the same way, l and l' are subequal.

Dividing (3) by (4), we can get:

$$\frac{I_{21}}{I_{11}} = \frac{C_2 - S_2}{C_1 - S_1}, \quad \textbf{(5)}$$

Substituting (1) and (2) into (5), we obtain:

$$e^{-u_1 d} = \frac{C_2 - S_2}{C_1 - S_1}, \quad \textbf{(6)}$$

$$S_1 = S_2 = \frac{C_2 - C_1 e^{-u_1 d}}{1 - e^{-u_1 d}} \quad \textbf{(7)}$$

Evaluation of scatter correction

Quantitative image quality parameters were analysed according to Ref.[18]. For the Contrast-to-noise ratio (CNR) two regions of interest (ROIs) at the same radius of the contrast-and-resolution phantom were analysed. The measured (denoted by the subscript M) mean values ($u_{M,1}, u_{M,2}$) and the standard deviations ($\sigma_{M,1}, \sigma_{M,2}$). The voxel noise ($\sigma_M$) is calculated as $\sigma_M = (\sigma_{M,1} + \sigma_{M,2})/2$ and the CNR was calculated as $CNR = \left|u_{M,1} - u_{M,2}\right| / \sigma_M$.

The magnitude of cupping $\tau_{cup} = 100(u_{M,edge} - u_{M,center}) / u_{M,edge}$ was extracted in terms of voxel values at the center $u_{M,center}$ and edge $u_{M,edge}$ of the water phantom.

The error of the CT number in the ROIs was calculated as the square root of the mean square error RMSE, defined as

$$E_{RMSE} = \sqrt{mean[(\mu_i - \overline{\mu_i})^2]},$$

where i is the index of the ROI, $\overline{\mu_i}$ is the mean reconstructed value in HU inside the ROI, and μ_i is the corresponding value measured in the ground-truth image.

EXPERIMENTS AND RESULTS

The tabletop CBCT systems and the SDB

The system parameters of the tabletop CBCT systems (figure 4) used in this work are summarized in TABLE 1. This system had geometries that were conceptually equivalent to that of clinical CBCT systems, except that the phantom was rotated, which provided an ideal circular trajectory. No bow-tie filter or anti-scatter grid was used on this system. We mounted the SDB on the outside surface of the collimator.

TABLE 1 : Imaging parameters of the physical experiments.

Parameters	System Value
X-ray focal spot	0.6 mm
X-ray energy	120 kVp,75mA
Detector size	TOSHIBA FXD4343R 430×439 mm^2 3008×3072 pixels
Source-to-imager distance	1400 mm
Source-to-object center distance	1000 mm
Source-to-SDB distance	230 mm
Anti-scatter grid	No
Bow-tie filter	No

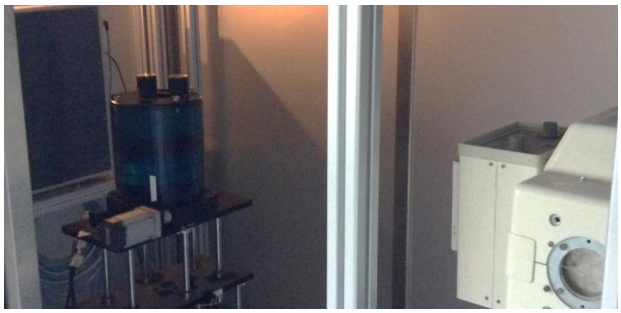

Figure 4 : The tabletop CBCT systems

Experiments on Phantom Ⅰ

Phantom Ⅰ is a 15mm iron wall plus 90mm-diameter aluminium cylinder. Figure 5 show the reconstructed images. As in Figure 5(a), the image distortion (cupping etc.) due to the scatter is obvious in the reconstructed images without scatter correction. The fan beam reconstruction show in Figure 5(b) is used as the reference. The scatter artifacts are greatly reduced in the images using the proposed method, which can be seen in the Figure 5(c).

The 1D horizontal profile with and without scatter signals can be seen in Figure 6. As in the figure, a reduction in the cupping artifacts when the image is corrected for scatter radiation is observed.

For a quantitative analysis of the reconstructed images, we measured the CNR and the magnitude of cupping in Figure 5(a). The results can be found in TABLE 2. Our approach increase the CNR from 1.75 to 2.35 and reduce the τ_{cup} from 42.3% to 1.3%. As show in TABLE 2, these artifacts are significantly suppressed when the proposed method is used with the SDB.

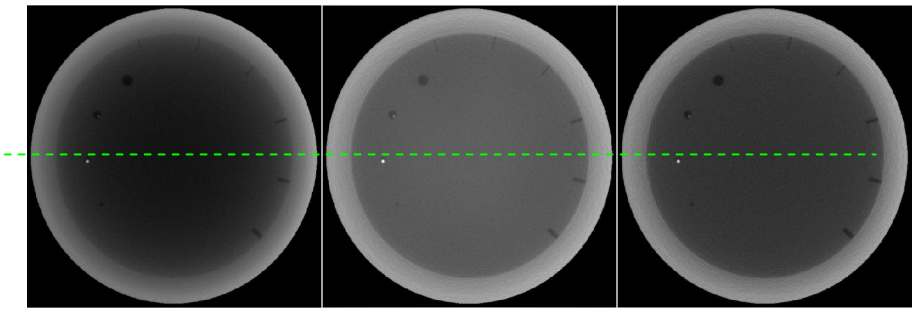

(a) **(b)** **(c)**

Figure 5 : Image reconstructions of the phantom. (a) CBCT without scatter correction; (b) CT acquired in fan beam geometry; (c) scatter correction using the SDB method.

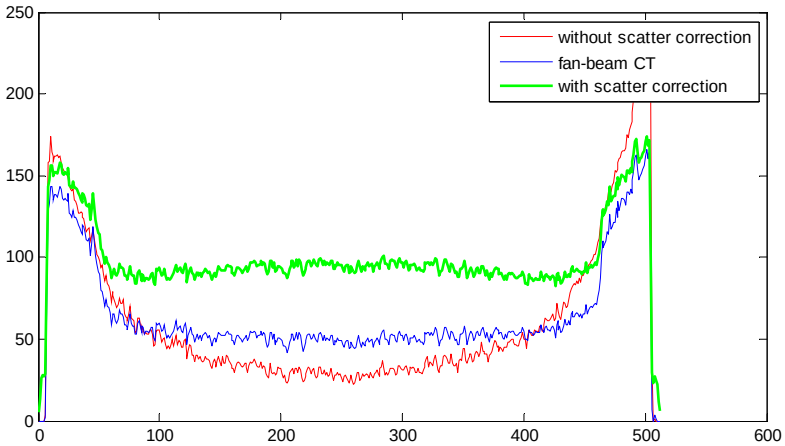

Figure 6 : The 1D horizontal profile of the measured and estimated scatter signals on the phantom: The column is the profiles of the projection images which is at row 256 in Figure 4.

TABLE 2 : Quantitative image quality investigation for the different modalities: CBCT without scatter correction (CBCT NONE), scatter correction using the SDB method (CBCT SC), fan beam geometry (FBCT). CNR and τ_{cup} are taken from the phantom.

Modality	τ_{cup} in[%]	Average CNR
CBCT NONE	42.3%	1.75
FBCT	0.5%	1.80
CBCT SC	1.3%	2.35

Experiments on Phantom Ⅱ:

The phantom Ⅱ is a 16cm×40cm×40cm cuboid solid water phantom. In this experiments, we only testify that SDB method can work well on projected image. As show in TABLE 3, Our approach reduce the τ_{cup} from 57.1% to 11.2% and can walk as well as Beam Stop Array (BSA) method which need two scan for one projected image.

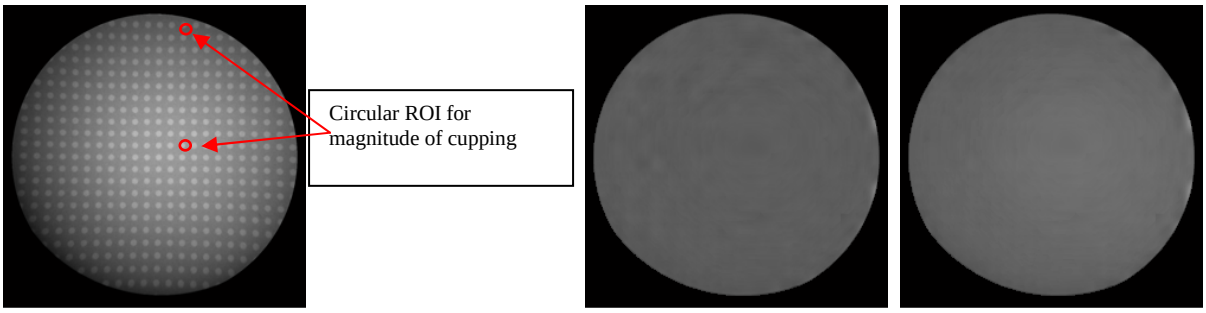

(a) **(b)** **(c)**

Figure7 : Projected image of the phantom Ⅱ. (a) CBCT without scatter correction; (b) BSA method; (c) scatter correction using the method. The selected as ROIs for CNR show in (a).

TABLE 3 : Quantitative image quality investigation for the different modalities: CBCT without scatter correction (CBCT NONE), CBCT with scatter correction (CBCT SC), fan beam geometry (FBCT). CNR and τ_{cup} are taken from the ROIs of the phantomⅡ.

Modality	E_{RMSE} (edge)	E_{RMSE} (center)	τ_{cup} in[%]
CB_NONE	1.64	1.32	57.1%
BSA	1.2	1.0	10.9%
CB_SC	0.6	0.4	11.2%

CONCLUSIONS

In this work, the improved scatter correction algorithm using SDB is evaluated using physical experiments on the phantom. The result shows that our algorithm produces substantial image quality improvements. Firstly, the proposed method reduces contrast-to-noise ratio of CBCT. Secondly, the magnitude of cupping is greatly descended. Our method easy to implement and without the loss of real-time imaging capabilities, which makes treatment planning using CBCT images a viable option.

ACKNOWLEDGMENT

The authors thank the anonymous referees for their constructive and insightful comments, which greatly improved the presentation. This work was sponsored by the Foundation Research Project of Jiangsu Province (The Natural Science Fund of Jiangsu Government, Grant No. BK20130883, BK20130868), NUPTSF (Grant No. NY213011) and NSF of China (Grant No. 61402239, 61401236)

REFERENCES

[1] J.Boone, J.Seibert; An analytical model of the scattered radiation distribution in diagnostic radiology, Med. Phys. **15(5)**, 721–725 **(1988)**.

[2] C.E.Floyd, A.H.Baydush, J.Y.Lo, J.E.Bowsher, C.E.Ravin; Scatter compensation for digital chest radiography using maximum likelihood expectation maximization, Invest. Radiol, **28(5)**, 427–433 **(1993)**.
[3] M.Honda, K.Kikuchi, K.Komatsu; Method for estimating the intensity of scattered radiation using a scatter generation model. Med. Phys., **18(2)**, 219–226 **(1991)**.
[4] J.Wiegert, M.Bertram, G.Rose, T.Aach; Model-based scatter correction for cone-beam computed tomography, Proc. SPIE, **5745**, 271-282 **(2005)**.
[5] D.G.Kruger, F.Zink, W.W.Peppler, D.L.Ergun, C.A.Mistretta; A regional convolution kernel algorithm for scatter correction in dualenergy images: Comparison to single-kernel algorithms, Med. Phys., **21(2)**, 175–184 **(1994)**.
[6] M.Zellerhoff, B.Scholz, E.P.Ruhrnschopf, T.Brunner; Low contrast 3D-reconstruction from C-arm data, Proc. SPIE. **5745**, 646–655 **(2005)**.
[7] R.Ning, X.Tang, D.Conover; X-ray scatter correction algorithm for cone-beam CT imaging, Med. Phys., **31(5)**, 1195–1202 **(2004)**.
[8] L.Zhu, N.Strobel, R.Fahrig; X-ray scatter correction for conebeam CT using moving blocker array, Proc. SPIE. **5745,** 251–258 **(2005)**.
[9] J.Boone; Scatter correction algorithm for digitally acquired radiographs: Theory and results. Med. Phys., **13(3),** 319–328 **(1986)**.
[10] A.Bani-Hashemi, E.Blanz, J.Maltz, D.Hristov, M.Svatos; Cone beam x-ray scatter removal via image frequency modulation and filtering. Med. Phys., **32(6),** 2093 **(2005)**.
[11] J.H.Siewerdsen, M.J.Daly, B.Bakhtiar, D.J.Moseley, S.Richard, H.Keller, et al.; A simple direct method for x-ray scatter estimation and correction in digital radiography and cone-beam CT. Med. Phys., **33(1),** 187–197 **(2006)**.
[12] L.Zhu, Y.Xie, J.Wang, L.Xing; Scatter correction method for X-ray CT using primary modulation: Theory and preliminary results. IEEE Trans. Med. Image., **25(12),** 1573-1587 **(2006)**.
[13] L.Zhu, J.Wang, L.Xing; Noise suppression in scatter correction for cone-beam CT, Medical Physics. **36(3)**, 741-752 **(2009)**.
[14] HUuDong-cai, Chen Hao Zhang, Ding-hua; Scatter Correction Method for Flat-Panel Detector-Based Cone Beam CT, Computerized Tomography Theory and Applications, **18(1)**, 16-22 **(2009)**.
[15] L.Spies, P.M.Evans, M.Partridge, V.N.Hansen, T.Bortfeld; Direct measurement and analytical modeling of scatter in portal imaging. Med. Phys., **27**, 462–471 **(2000)**.
[16] C.Jonsson, S.A.Larsson; A spatially varying Compton scatter correction for SPECT utilizing the integral Klein-Nishina cross section. Phys. Med. Biol. **46,** 1767–1783 **(2001)**.
[17] E.Spezi, P.Downes, E.Radu, R.Jarvis; Monte Carlo simulation of an x-ray volume imaging cone beam CT unit. Medical Physics. **36(1),** 127-136 **(2009)**.
[18] J.H.Siewerdsen, D.A.Jaffray; Cone-beam computed tomography with a flat-panel imager: magnitude and effects of X-ray scatter. Med. Phys., **28(2),** 220-231 **(2001)**.